Mono- and Dinuclear Transition Metal Complexes of the Hexadentate Ligand Tris(4-*tert*-butyl-2-mercaptobenzyl)-1,4,7-triazacyclononane (L)

Thomas Beissel,[1a] Thorsten Glaser,[1a] Frank Kesting,[1a] Karl Wieghardt,*[,1a] and Bernhard Nuber[1b]

Max-Planck-Institut für Strahlenchemie, D-45470 Mülheim an der Ruhr, Germany, and Anorganisch-Chemisches Institut der Universität, D-69120 Heidelberg, Germany

Received December 19, 1995[⊗]

The hexadentate, pendant arm macrocycle 1,4,7-tris(4-*tert*-butyl-2-mercaptobenzyl)-1,4,7-triazacyclononane (H_3L) has been synthesized and isolated as its trihydrochloride, $H_3L\cdot 3HCl$, or sodium salt, Na_3L, and its coordination chemistry with first-row transition metals has been studied. Mononuclear complexes of the type $[LM^{III}]$ (M = Ga (**1**), In (**2**), V (**3**), Cr (**4**), Mn (**5**), Fe,Co (**6**)) have been isolated as have the one-electron-oxidized forms $[LM]PF_6$ (M = V^{IV} (**3a**), Mn^{IV} (**5a**)). The crystal structure of **6** has been determined by single-crystal X-ray crystallography. Complex **6** crystallizes in the orthorhombic space group *Iba2*, with cell constants $a = 14.206(8)$ Å, $b = 22.53(1)$ Å, $c = 26.07(1)$ Å, $V = 8344.0(3)$ Å^3, and $Z = 8$. The cobalt(III) ion is in a distorted octahedral *fac*-N_3S_3 donor set. The reaction of L with divalent metal chlorides in a 1:2 ratio in methanol affords the homodinuclear complexes $[LM^{II}_2Cl]$ (M = Mn (**7**), Co (**8**), Ni (**9**), Zn (**10**), Cd (**11**)) where one metal is six-(N_3MS_3) and the other is four-coordinate (S_3MCl); the two polyhedra are linked by three μ_2-thiolato bridges. Heterodinuclear complexes of the type $[LM^1M^2Cl]$ have been obtained from $[LM_2Cl]$ species by abstraction of the four-coordinate metal ion and replacement by a different metal ion. The complexes $[LZn^{II}M^{II}Cl]$ (M = Fe (**12**), Co (**13**), Ni (**14**)), $[LNi^{II}M^{II}Cl]$ (M = Co (**15**), Zn (**16**)), and $[LMn^{II}M^{II}Cl]$ (M = Fe (**17**), Co (**18**), Ni (**19**), Zn (**20**), Cd (**21**), Hg (**22**)) have been isolated as solid materials. The crystal structure of **14** has been determined by X-ray crystallography. Complex **14** crystallizes in the orthorhombic space group $P2_12_12_1$, with cell constants $a = 15.45(1)$ Å, $b = 17.77(1)$ Å, $c = 17.58(1)$ Å, $V = 4826.5(4)$ Å^3, and $Z = 4$. The linkage isomers **14** and **16** show characteristic electronic spectra for octahedrally and tetrahedrally coordinated Ni(II), respectively. The electronic structures of new complexes have been investigated by UV−vis spectroscopy; their magnetochemistry and electrochemistry are reported.

Introduction

N-Functionalization of the tridentate macrocycle 1,4,7-triazacyclononane with organic entities carrying an additional functional group generates hexadentate ligands[2] which, in general, very strongly bind to divalent and trivalent transition metal ions. In a few instances, very large stability constants have been measured; e.g., the tris(*o*-hydroxybenzyl) derivatives I[3−7] have been shown to bind to iron(III) even more strongly

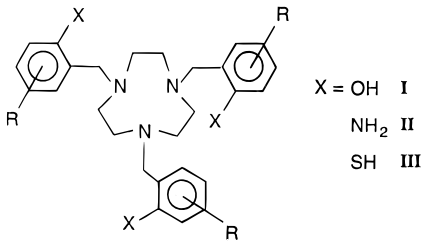

than natural siderophores.[8−10] Recently we substituted the OH group in I by an NH_2 group, affording a type II ligand.[11−13] 1,4,7-Tris(*o*-aminobenzyl)-1,4,7-triazacyclononane also binds strongly to di- or trivalent metal ions[11−13] as does the ligand 1,4,7-tris(4-*tert*-butyl-2-mercaptobenzyl)-1,4,7-triazacyclononane (type III), whose iron(III) complex $[LFe^{III}]$ has been briefly communicated.[14]

Ligands of types I−III offer some unique opportunities in coordination chemistry. The inherent enormous stability of the mononuclear six-coordinate complexes has allowed a detailed ligand field spectroscopic investigation of C_3 symmetric species containing a facial N_3O_3, $N_3(NH_2)_3$ vs $N_3(NH)_3$, or N_3S_3 donor set. Furthermore, a given complex may exist in different oxidation states and interesting redox chemistry may evolve where the ligand-enforced thermodynamic stability of the oxidized or reduced species allows a detailed study of these complexes. Metal- *versus* ligand-centered redox processes can be detected. For example, photogeneration of a coordinated phenoxyl radical was recently demonstrated for some tris(phenolato)iron(III) complexes.[15]

⊗ Abstract published in *Advance ACS Abstracts,* June 1, 1996.

(1) (a) Max-Planck-Institut. (b) Universität Heidelberg.
(2) Chaudhuri, P.; Wieghardt, K. *Prog. Inorg. Chem.* **1987**, *35*, 329.
(3) Moore, D. A.; Fanwick, P. E.; Welch, M. J. *Inorg. Chem.* **1989**, *28*, 1504.
(4) Auerbach, U.; Eckert, U.; Wieghardt, K.; Nuber, B.; Weiss, J. *Inorg. Chem.* **1990**, *29*, 938.
(5) Auerbach, U.; Weyhermüller, T.; Wieghardt, K.; Nuber, B.; Bill, E.; Butzlaff, C.; Trautwein, A. X. *Inorg. Chem.* **1993**, *32*, 508.
(6) Auerbach, U.; Della Vedova, B. S. P. C.; Wieghardt, K.; Nuber, B.; Weiss, J. *J. Chem. Soc., Chem. Commun.* **1990**, 1004.
(7) Auerbach, U.; Stockheim, C.; Weyhermüller, T.; Wieghardt, K.; Nuber, B. *Angew. Chem., Int. Ed. Engl.* **1993**, *32*, 714.
(8) Martell, A. E.; Motekaitis, R. J.; Welch, M. J. *J. Chem. Soc., Chem. Commun.* **1990**, 1748.
(9) Clarke, E. T.; Martell, A. E. *Inorg. Chim. Acta* **1991**, *186*, 103.
(10) Motekaitis, R. J.; Sun, Y.; Martell, A. E. *Inorg. Chim. Acta* **1992**, *198−200*, 421.
(11) Schlager, O.; Wieghardt, K.; Grondey, H.; Rufinska, A.; Nuber, B. *Inorg. Chem.* **1995**, *34*, 6440.
(12) Schlager, O.; Wieghardt, K.; Nuber, B. *Inorg. Chem.* **1995**, *34*, 6449.
(13) Schlager, O.; Wieghardt, K.; Nuber, B. *Inorg. Chem.* **1995**, *34*, 6456.
(14) Beissel, T.; Bürger, K.-S.; Voigt, G.; Wieghardt, K. *Inorg. Chem.* **1993**, *32*, 124.
(15) Hockertz, J.; Steenken, S.; Wieghardt, K.; Hildebrandt, P. *J. Am. Chem. Soc.* **1993**, *115*, 11222.

S0020-1669(95)01623-5 CCC: $12.00

Scheme 1. Synthesis of the Ligand $H_3L \cdot 3HCl$

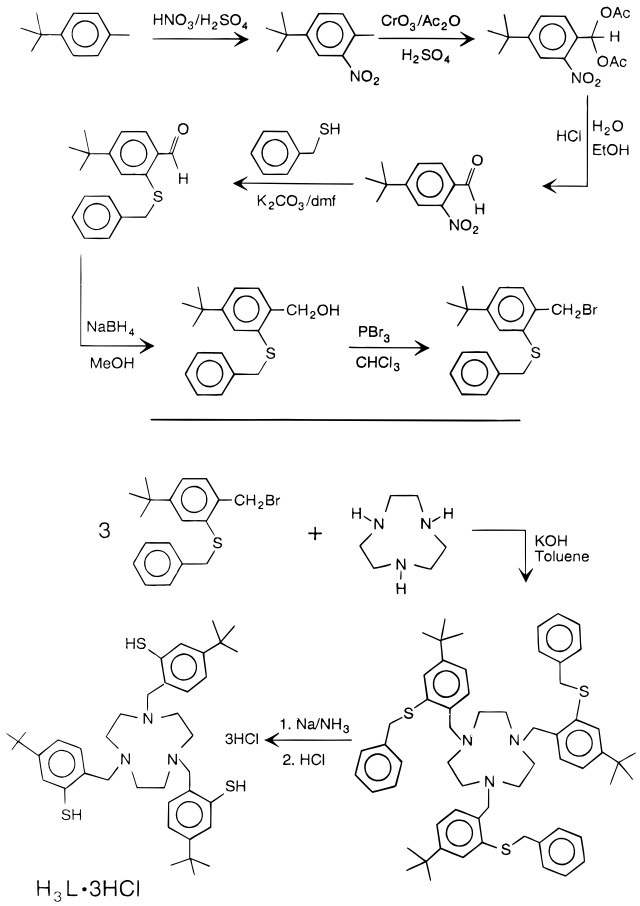

Due to the fact that these ligands enforce a stereochemical arrangement of the three pendant arm functionalities in *cis* positions relative to each other, the mononuclear complexes can themselves act as ligands for further covalent binding of transition metal ions and oligonuclear complexes may thus be formed. The heterotrinuclear species bis[(1,4,7-tris(5-*tert*-butyl-2-hydroxybenzyl)-1,4,7-triazacyclononane)cobalt(III)]iron(II) diperchlorate has been characterized by X-ray crystallography.[7] Here the phenolates form six μ_2 bridges between the cobalt(III) and iron(II) ions.

Thiolates are well-known to form bridges between transition metal ions. Therefore, we decided to study the coordination chemistry of the tris(thiophenolato) ligand 1,4,7-tris(4-*tert*-butyl-2-mercaptobenzyl)-1,4,7-triazacyclononane (H_3L) in depth. Here we report its synthesis (Scheme 1) and a series of mono- and dinuclear complexes. Its remarkable ability to bind even to sodium and to form trinuclear complexes was recently shown by the synthesis of the complex [$LNaRu^{IV}NaL$] and its osmium(IV) analogue.[16]

Experimental Section

The ligand 1,4,7-triazacyclononane was prepared according to a published procedure.[17]

Synthesis of the Ligand $H_3L \cdot 3HCl$. The synthesis of the ligand is schematically shown in Scheme 1. Preparation of 4-*tert*-butyl-2-nitrotoluene was achieved by the reaction of 4-*tert*-butyltoluene (300 g) and a mixture of HNO_3 (68%, 195 mL) and H_2SO_4 (96%, 240 mL), which was added dropwise with stirring and efficient cooling (0−5 °C) to the toluene derivative. The resulting solution was stirred for 3 h at 0−5 °C, after which the solution was carefully added to water (1 L) at 0 °C. This solution was extracted with diethyl ether (three times with 400 mL). The combined ether phases were washed with a saturated aqueous $NaHCO_3$ solution (100 mL), dried over $MgSO_4$, and filtered. After removal of the solvent by rotary evaporation, a yellow oil was obtained (yield: 371 g, 95%).

The crude oil (100 g) was subsequently dissolved in acetic acid anhydride (500 mL), the solution was cooled in an ice/NaCl bath to −5 °C, and concentrated H_2SO_4 (80 mL) was added dropwise with vigorous stirring and efficient cooling (0 °C). A freshly prepared and cooled solution of CrO_3 (160 g) in acetic acid anhydride (400 mL) was then added dropwise to the above reaction mixture with efficient cooling. (*Caution:* CrO_3 was added in small amounts with efficient cooling only to the acetic acid anhydride. The resulting solution must not come into contact with oxidizable substances (explosion).) The temperature should at no time exceed 5 °C. After the solutions were combined, stirring was continued for 2 h. The resulting mixture was slowly added to water (6 L) at 2 °C. This solution was extracted twice with diethyl ether (1 L at each time). After separation and recovery of the organic phase, it was washed with H_2O two to three times and then with a saturated aqueous $NaHCO_3$ solution (neutralization). The deep brown ether phase was dried over $MgSO_4$, and the solvent was removed by rotary evaporation. A brown oil of crude 4-*tert*-butyl-2-nitrobenzaldehyde diacetate was obtained. Yield: 105 g (70%).

The unprotected aldehyde was prepared by hydrolysis of the above crude oil dissolved in ethanol (160 mL) in a mixture of concentrated HCl (470 mL) and water (650 mL). The mixture was heated to reflux for 2 h. The cooled solution was added to water (1.5 L) at 0 °C, and the mixture was stirred for a few minutes. Extraction of this phase with diethyl ether (two times with 1 L of diethyl ether) and its workup as described above produced a dark brown oil (yield: 70 g, ∼98%).

This crude material was used for the preparation of 4-*tert*-butyl-2-(benzylthio)benzaldehyde. A 70 g quantity of the above product was dissolved in dimethylformamide (dmf) (80 mL), and K_2CO_3 (70 g) was added. Subsequently, benzyl mercaptan (40 mL) was added to this solution (*caution:* use hood). This reaction mixture was stirred at 80 °C for 12 h in a sealed vessel. After cooling, the solution was added to water (1 L) at 0 °C and extracted with diethyl ether. The workup of the organic phase was as described above. A brown-red oil was obtained (yield: 87 g, 88%).

Conversion of the aldehyde to the corresponding alcohol was achieved by reduction of a methanolic solution (200 mL) of the above crude aldehyde (87 g) with $NaBH_4$ (7.4 g) which was added in small amounts with stirring for 2 h at 0 °C. The solvent was stripped by rotary evaporation, and the residue was quickly dissolved in diethyl ether. The diethyl ether phase was washed with water (two or three times), dried over $MgSO_4$, and filtered, and the solvent was removed by rotary evaporation. The oily brown residue was stored for 5 days at 0 °C, during which the alcohol crystallized in ∼66% yield. The crystals were filtered off and washed with cold *n*-heptane. This product is stable toward air and can be stored for months.

Conversion of the alcohol to the corresponding bromide was carried out by reaction of the above crude alcohol (30 g) dissolved in $CHCl_3$ (150 mL) and with $CHCl_3$ solution (100 mL) of PBr_3 (11.0 g) at 0 °C. The combined solutions were stirred at 0 °C for 30 min, after which water (250 mL) was added. The organic phase was repeatedly washed with water until the pH of the water remained neutral. This procedure should be carried out as quickly as possible since the bromide is not very stable in solution. The washed organic phase was dried over $MgSO_4$ and filtered. Removal of the solvent produced a pale yellow viscous solution from which, upon cooling to −10 °C for a few hours, a yellow crystalline material of 2-(benzylthio)-4-*tert*-butylbenzyl bromide precipitated. Yield: 33 g (∼90%).

To a solution of 1,4,7-triazacyclononane (4.5 g) in toluene (100 mL) was slowly added a solution of the above 2-(benzylthio)-4-*tert*-butylbenzyl bromide (33 g) in toluene (100 mL). After addition of finely powdered KOH (5.3 g), the solution was stirred at 80 °C for 12 h. The cooled and filtered solution was dried over $MgSO_4$, and after filtration, the solvent was stripped off by rotary evaporation, yielding 32 g (∼90%) of an orange-yellow, viscous oil. This material was dissolved in degassed tetrahydrofuran (70 mL), and the solution was

(16) Mochizuki, K.; Kesting, F.; Weyhermüller, T.; Wieghardt, K.; Butzlaff, C.; Trautwein, A. X. *J. Chem. Soc., Chem. Commun.* **1994**, 909.
(17) Wieghardt, K.; Schmidt, W.; Nuber, B.; Weiss, J. *Chem. Ber.* **1979**, *112*, 2220.

added dropwise to liquid ammonia (200 mL) under a dinitrogen blanketing atmosphere with stirring.

To this solution were added small amounts (pieces) of metallic sodium (5 g) with vigorous stirring, whereupon the color of the solution changed to green. After the sodium had completely dissolved, solid NH_4Cl was added to remove any excess Na. The ammonia was now allowed to slowly evaporate by gently heating the solution to 20 °C. The yellow residue contains mainly Na_3L and can be used for the synthesis of complexes; it is very air-sensitive and must be stored under argon. In order to convert the sodium salt into the more stable form $H_3L \cdot 3HCl$, the residue was dissolved in degassed diethyl ether (200 mL) to which degassed 1.0 M concentrated aqueous HCl (200 mL) had been added. The combined solutions under an argon atmosphere were vigorously shaken. Then the aqueous phase was removed and discarded. The ether phase was dried over $MgSO_4$ under argon. Upon removal of the solvent by evaporation in vacuo, the protonated ligand $H_3L \cdot 3HCl$ precipitated as light-yellow material. Yield: 24 g.

It is important to notice that deprotection of the mercapto group gives very oxygen-sensitive materials. Exclusion of air is essential for good yields. The final product $H_3L \cdot 3HCl$ is not as air-sensitive as the Na_3L intermediate and can be stored in the solid state for months without noticeable decomposition under argon. The crude product $H_3L \cdot 3HCl$ was used for the syntheses of complexes without further characterization or purification. The fast atom bombardment (FAB) mass spectrum revealed the molecular ion $[LH_4]^+$ peak at $m/z = 664.4$ (100%) (calcd 664.0).

Preparation of Mononuclear Complexes. [LGa^{III}] (1) and [Lln^{III}] (2). To an argon-purged solution of methanol (40 mL) and triethylamine (2 mL) was added the ligand $H_3L \cdot 3HCl$ (0.49 g, 0.63 mmol). $Ga(NO_3)_3 \cdot xH_2O$ (0.16 g, 0.63 mmol) or $InCl_3$ (0.14 g; 0.63 mmol) were added to the clear yellow solution which was heated to reflux for 90 min. During this procedure and after cooling to 5 °C, colorless precipitates of **1** and **2** formed in ~60% yields. 80 MHz ^{1}H NMR spectrum of **1** ($CDCl_3$): $\delta = 1.22$ (s, $-CH_3$, 27 H), 2.40−3.17 (m, $-CH_2CH_2-$, 12 H), 3.30 (d, RCH_2N, 3 H), 5.35 (d, RCH_2N, 3 H), 6.88 (s, aromatic protons, 3 H), 7.24 (s, aromatic protons, 3 H), 7.36 (s, aromatic protons, 3 H).

[LV^{III}] (3). The ligand $H_3L \cdot 3HCl$ (0.67 g; 0.87 mmol) was added to an argon-purged solution of methanol (40 mL) and NEt_3 (0.5 mL); $V^{II}(SO_4) \cdot 6H_2O$ (0.22 g, 0.87 mmol) was added under strictly anaerobic conditions. The solution was heated to reflux for 3 h. After the yellow-brown solution was cooled to 20 °C, it was briefly stirred in the presence of air until a red-violet microcrystalline precipitate of **3** formed in 32% yield.

[LV^{IV}]PF$_6$ (3a). To a solution of **3** (0.20 g, 0.28 mmol) in acetone (20 mL) was added ferrocenium hexafluorophosphate, $[Fc]PF_6$, (93 mg, 0.28 mmol). The solution was stirred under argon at 20 °C for 30 min, and its volume was reduced to one-third by evaporation of the solvent. Addition of diethyl ether (40 mL) initiated the precipitation of deep violet microcrystals of **3a**.

[LCr^{III}] (4). $Cr^{II}_2(acetate)_4 \cdot 2H_2O$ (0.11 g, 0.32 mmol) was added under an argon blanketing atmosphere to a degassed solution of $H_3L \cdot 3HCl$ (0.50 g, 0.65 mmol) and NEt_3 (0.5 mL) in methanol (40 mL). The suspension was heated to reflux for 2 h, during which a light-green precipitate of **4** formed. This suspension was briefly stirred in the presence of air to ensure complete oxidation to chromium(III). Yield: ~70%.

[LMn^{III}] (5). To a degassed solution of the ligand $H_3L \cdot 3HCl$ (0.66 g, 0.85 mmol) in methanol (30 mL) and NEt_3 (2 mL) was added $[Mn^{III}_3(acetate)_6O][acetate]$ (0.20 g, 0.34 mmol). The solution was cooled to 0 °C and stirred under an argon atmosphere for 40 min, during which a yellow-brown precipitate of **5** formed in 25% yield. This material is very air-sensitive (color change to green) both in the solid state and in solution.

[LMn^{IV}]PF$_6$ (5a). $[Fc]PF_6$ (41 mg; 0.12 mmol) was dissolved in degassed acetone (30 mL) to which **5** (87 mg, 0.12 mmol) had been added. The solution was stirred at 20 °C for 30 min and filtered. The solvent was removed by evaporation, and the green residue was washed several times with diethyl ether to remove the ferrocene. The green microcrystals of **5a** (yield: 60%) are stable in the solid state, but solutions of **5a** decompose rapidly.

[LCo^{III}] (6). To a degassed solution of $H_3L \cdot 3HCl$ (0.50 g, 0.65 mmol) in methanol (40 mL) and NEt_3 (0.5 mL) was added $CoCl_2 \cdot 6H_2O$ (0.15 g, 0.65 mmol). The solution was heated to reflux in the absence of air for 1 h, after which a gray precipitate of **6** formed in 64% yield. This material contains small amounts of a trinuclear species, $[L_2Co^{III}_3]Cl_3$, which was removed by extraction with hot methanol (40 mL).

Preparation of Homodinuclear Complexes. [LM$^{II}_2$Cl]. The homodinuclear complexes containing the divalent transition metal ions Mn (**7**), Co (**8**), Ni (**9**), Zn (**10**), and Cd (**11**) were synthesized according to the following general procedure.

To a degassed solution of the ligand $H_3L \cdot 3HCl$ (1.0 g; 1.3 mmol) and $[NEt_4]Cl$ (0.5 g) in methanol (80 mL) and NEt_3 (2.0 mL) was added 3.0 mmol of the corresponding metal dichloride hydrate or acetate ($MnCl_2 \cdot 4H_2O$; $CoCl_2 \cdot 6H_2O$; $NiCl_2 \cdot 6H_2O$; $Zn(acetate)_2$; $CdCl_2 \cdot 6H_2O$). Under strictly anaerobic conditions (argon atmosphere), these solutions were heated to reflux for 30 min, during which microcrystalline precipitates of colorless **7**, green **8**, green-brown **9**, colorless **10**, and colorless **11** formed, respectively. Complex **7** is very air-sensitive both in the solid state and in solution and can only be stored without decomposition at temperatures <0 °C. The yields vary in all cases between 30 and 45%.

Preparation of Heterodinuclear Complexes. The heterodinuclear complexes $[LM^1M^2Cl]$ were synthesized according to either of the two methods described below.

Method A. To a solution of tetraethylammonium chloride (0.5 g) and 1,4,7-triazacyclononane (62 mg, 0.48 mmol) in degassed methanol (40 mL) was added $[LZn_2Cl]$ **10** (0.20 g, 0.24 mmol). The suspension was heated to 50 °C under an argon blanketing atmosphere for 20 min. To the cooled (20 °C), clear, colorless solution was added dropwise a solution of $FeCl_2 \cdot 6H_2O$ (60 mg), $CoCl_2 \cdot 6H_2O$ (60 mg), or $NiCl_2 \cdot 6H_2O$ (60 mg) in methanol (15 mL). Upon stirring, microcrystalline precipitates of **12**−**14** formed, respectively, within a few minutes in ~80% yields: **12**, pale yellow; **13**, green; **14**, brick red.

Complexes **15** and **16** were prepared analogously by using $[LNi_2Cl]$, **9**, as starting material. Addition of $Zn(acetate)_2$ to a solution of **9** afforded green microcrystals of **16** whereas with $CoCl_2 \cdot 6H_2O$ green crystals of **15** were obtained.

Method B. The complex $[LMn]^-$ was prepared *in situ* under strictly anaerobic conditions (argon): To a solution of $H_3L \cdot 3HCl$ (0.30 g, 0.39 mmol) in methanol (50 mL) and NEt_3 (2 mL) was added $MnCl_2 \cdot 4H_2O$ (77 mg, 0.39 mmol). The yellow solution was heated to reflux for 10 min. It is noted that because $H_3L \cdot 3HCl$ is always contaminated with—at least some—NH_4Cl, the above procedure also gives some **7** which may precipitate at this point. To this solution was added dropwise methanolic solutions (15 mL) of 0.4 mmol of $FeCl_2 \cdot 6H_2O$, $CoCl_2 \cdot 6H_2O$, $Ni(acetate)_2 \cdot 4H_2O$, $Zn(acetate)_2$, $CdCl_2 \cdot H_2O$, and $HgCl_2$, respectively, under strictly anaerobic conditions. Within a few minutes, precipitates formed, which were collected by filtration, washed with diethyl ether, and dried under argon. The following crystalline materials were obtained in 50−70% yields: pale-brown **17**, gray-green **18**, green **19**, colorless **20**−**22**.

All new complexes gave satisfactory elemental analyses, the results of which are available in the Supporting Information (Table S1).

Physical Measurements. Electronic absorption spectra were measured in the range 250−1500 nm on a Perkin-Elmer Lambda 9 spectrophotometer. The 400 MHz ^{1}H NMR spectra were recorded on a Bruker AM 400 FT spectrometer at a magnetic field of 400.13 MHz with the solvent as internal standard. The magnetic susceptibilities of powdered samples of complexes were measured either in the temperature range 80−293 K by using the Faraday method or in the range 2−293 K on a SQUID magnetometer (MPMS, Quantum Design). The diamagnetism of the sample was taken into account by using Pascal's constants. Cyclic voltammetric measurements were carried out by use of PAR equipment (M173 potentiostat; M175 universal programmer) on solutions containing 0.10 M tetra-*n*-butylammonium hexafluorophosphate as supporting electrolyte. Potentials are referenced to the Ag/AgCl electrode (saturated LiCl in ethanol) at ambient temperature. The ferrocenium/ferrocene (Fc^+/Fc) couple was used as internal standard ($\approx 10^{-5}$ M). Under our experimental conditions, the Fc^+/Fc couple is at $E_{1/2} = +0.51$ V vs Ag/AgCl.

Table 1. Crystallographic Data for [LCo^{III}] (**6**) and [LZnNiCl]·2C_3H_6O (**14**)

	6	**14**
formula	$C_{39}H_{54}CoN_3S_3$	$C_{45}H_{66}N_3NiO_2S_3Zn$
fw	720.0	901.32
cryst syst	orthorhombic	orthorhombic
space group	*Iba*2 (No. 45)	$P2_12_12_1$ (No. 19)
a, Å	14.206(8)	15.45(1)
b, Å	22.53(1)	17.77(1)
c, Å	26.07(1)	17.58(1)
V, Å^3	8344.0(3)	4826.5(4)
Z	8	4
ρ_{calc}, g cm^{-3}	1.29	1.29
F(000)	3072	1984
μ, mm^{-1}	1.15	1.12
cryst dimens, mm	0.1 × 0.1 × 0.6	0.08 × 0.1 × 0.9
abs cor	empirical (ψ scans)	empirical (ψ scans)
λ, Å	0.710 73	0.710 73
T, °C	20	20
no. of total data collected	2180	4976
no. of unique obsd data	843	2426
no. of parameters refined	204	506
R^a	0.081	0.059
$R_w{}^b$	0.068	0.046
largest residual electron density, e Å^{-3}	0.59	0.46

^{a} $R = \sum(|F_o| - |F_c|)/\sum|F_o|$. ^{b} $R_w = [\sum w(|F_o| - |F_c|)^2/\sum w|F_o|^2]^{1/2}$; $w^{-1} = \sigma^2(F) + 0.0001F^2$.

Fast atom bombardment mass spectrometry (liquid secondary ion mass spectrometry) was performed on solid samples dispersed in a *m*-nitrobenzaldehyde matrix.

X-ray Crystallography. The crystallographic data on [LCo^{III}] (**6**) and [LZnNiCl]·2(acetone) (**14**) are summarized in Table 1. A black needle-shaped crystal of **6** and a red needle-shaped crystal of **14** were placed on a Siemens AED II and a Syntex R3 diffractometer, respectively. Graphite-monochromated Mo Kα X-radiation was used throughout. Intensity data were corrected for Lorentz, polarization, and absorption effects (ψ scans) in the usual manner. The structures were solved by conventional Patterson and difference Fourier methods by using the SHELXTL-PLUS program package.[18] The function minimized during full-matrix least-squares refinement was $\sum w(|F_o| - |F_c|)^2$, where $w^{-1} = \sigma^2(F)$. Neutral-atom scattering factors and anomalous dispersion corrections for non-hydrogen atoms were taken from ref 19. The hydrogen atoms in **14** were placed at calculated positions with isotropic thermal parameters; the methyl groups were treated as rigid bodies. All-hydrogen atoms in **14** were refined with anisotropic thermal parameters. Due to the presence of three *tert*-butyl groups per Co in **6**, the crystallinity of the crystal was not as good as desirable for a high-quality X-ray determination. At higher reflection angles, the intensity of reflections quickly deteriorated and, consequently, the data-to-parameter ratio was very low. Therefore, only the Co and S atoms of **6** were refined with anisotropic thermal parameters. The data:parameter ratio is still very low, 4.13:1, and the structure determination of **6** can only serve to demonstrate the expected atom connectivity. Since **6** crystallizes in a noncentrosymmetric space group, Roger's[20a] η factor test and Hamilton's *R* test[20b] were carried out, which proved to be inconclusive. Therefore, the structure was fully refined in both enantiomeric forms and the refinement yielding the lower *R* value was deemed to be the correct one. Atom coordinates for **6** and **14** are listed in Tables 2 and 3, respectively.

(18) Full-matrix least-squares structure refinement program package Siemens SHELXTL-PLUS: G. M. Sheldrick (University of Göttingen).
(19) *International Tables of Crystallography*; Kynoch: Birmingham, England, 1974; Vol. IV, pp 99, 149.
(20) (a) Roger, D. *Acta Crystallogr*. **1981**, *A37*, 734. (b) Hamilton, W. C. *Ibid*. **1965**, *18*, 502.

Table 2. Atomic Coordinates (×10^4) and Equivalent Isotropic Displacement Parameters (Å^2 × 10^3) for **6**

	x	*y*	*z*	*U*(eq)^a
Co(1)	888(3)	7015(3)	2502(3)	46(2)
S(1)	1908(9)	6448(7)	2061(5)	48(6)
S(2)	1864(10)	7757(6)	2299(4)	51(6)
S(3)	1888(8)	6850(6)	3141(4)	43(5)
N(1)	−8(24)	6363(15)	2723(12)	24(10)
N(2)	23(23)	7139(18)	1869(12)	48(11)
N(3)	81(36)	7564(20)	2917(17)	87(17)
C(1)	−649(26)	6255(17)	2309(13)	22(13)
C(2)	−398(31)	6546(20)	1816(17)	49(18)
C(3)	−817(30)	7579(18)	2044(16)	41(13)
C(4)	−423(33)	7936(18)	2448(22)	76(18)
C(5)	−738(26)	7187(18)	3175(15)	52(16)
C(6)	−407(31)	6545(20)	3180(17)	46(18)
C(7)	469(27)	5776(19)	2803(16)	54(16)
C(8)	439(28)	7371(19)	1407(17)	63(18)
C(9)	531(30)	7978(21)	3302(18)	67(17)
C(10)	1536(36)	5720(20)	2049(19)	61(16)
C(11)	1912(35)	5358(18)	1690(16)	39(14)
C(12)	1753(35)	4763(20)	1621(18)	65(15)
C(13)	1024(31)	4524(21)	1936(18)	79(17)
C(14)	654(26)	4891(20)	2286(15)	48(14)
C(15)	879(32)	5454(19)	2345(16)	51(14)
C(16)	1461(29)	8186(18)	1792(16)	33(13)
C(17)	1843(42)	8740(20)	1721(20)	78(19)
C(18)	1591(41)	9116(22)	1303(19)	78(16)
C(19)	1010(28)	8891(17)	883(17)	61(14)
C(20)	578(26)	8320(19)	983(16)	47(14)
C(21)	848(32)	7983(20)	1393(19)	56(15)
C(22)	1611(28)	7214(16)	3686(14)	34(12)
C(23)	1937(23)	7015(23)	4164(14)	56(12)
C(24)	1691(36)	7344(20)	4634(18)	80(16)
C(25)	826(33)	7783(21)	4698(20)	103(18)
C(26)	626(28)	7978(20)	4231(18)	62(15)
C(27)	887(31)	7689(20)	3774(15)	47(13)
C(28)	2302(55)	4411(30)	1207(25)	128(28)
C(29)	2010(40)	3787(23)	1256(21)	151(27)
C(30)	2011(39)	4572(22)	700(21)	172(29)
C(31)	3509(39)	4458(24)	1347(21)	150(26)
C(32)	2113(60)	9750(32)	1225(29)	139(27)
C(33)	2319(39)	10045(24)	1768(19)	142(23)
C(34)	1611(54)	10058(41)	880(33)	402(73)
C(35)	3093(48)	9661(31)	989(28)	271(51)
C(36)	2267(45)	7208(29)	5107(31)	167(30)
C(37)	3172(39)	6842(29)	5063(23)	234(37)
C(38)	2153(44)	7430(26)	5554(20)	165(29)
C(39)	1888(49)	6489(33)	5221(31)	407(32)

^{a} Equivalent isotropic *U* defined as one-third of the trace of the orthogonalized $\mathbf{U}_{ij}$ tensor.

Results

Syntheses. The synthetic route to the ligand 1,4,7-tris(4-*tert*-butyl-2-mercaptobenzyl)-1,4,7-triazacyclononane, H_3L, as its trihydrochloride, H_3L·3HCl, or its sodium salt, Na_3L, is depicted in Scheme 1, and Chart 1 shows the complexes prepared. The sodium salt is very air-sensitive both in the solid state and in solution and must be stored under an argon or dinitrogen atmosphere. The trihydrochloride is relatively more stable toward oxygen in the solid state but was also kept under an argon blanketing atmosphere.

Reaction of a methanolic solution of H_3L·3HCl, to which an excess of triethylamine was added, with $Ga(NO_3)_3$·xH_2O or $InCl_3$ at elevated temperatures produced colorless microcrystals of [LGa^{III}] (**1**) and [LIn^{III}] (**2**), respectively. Using $V(SO_4)$·$6H_2O$ as starting material and otherwise identical reaction conditions under argon produced a yellow-brown solution which, upon exposure to air, became red-violet, and microcrystalline red-violet [LV^{III}] (**3**) precipitated. Oxidation of **3** in acetone with 1 equiv of ferrocenium hexafluorophosphate ([Fc]PF_6) under argon afforded a deep-violet precipitate of [LV^{IV}]PF_6 (**3a**).

Table 3. Atomic Coordinates ($\times 10^4$) and Equivalent Isotropic Displacement Parameters ($Å^2 \times 10^3$) for **14**

	x	*y*	*z*	*U*(eq)[a]
Ni(1)	8546(1)	1789(1)	8061(1)	47(1)
S(1)	8952(2)	3038(2)	7893(2)	44(1)
S(2)	7552(2)	2107(2)	9006(2)	41(1)
S(3)	9641(2)	1545(2)	8939(2)	44(1)
Cl(1)	8346(3)	1003(3)	7112(3)	104(2)
Zn(1)	8953(1)	2804(1)	9343(1)	37(1)
N(1)	9914(7)	3726(5)	9441(6)	33(4)
N(2)	8147(7)	3639(5)	9994(6)	35(4)
N(3)	9408(7)	2579(6)	10514(6)	39(4)
C(1)	9500(9)	4412(7)	9786(8)	50(6)
C(2)	8502(9)	4371(8)	9699(8)	47(6)
C(3)	8305(9)	3551(8)	10828(7)	44(6)
C(4)	8657(8)	2758(8)	10989(7)	42(5)
C(5)	10170(8)	3082(7)	10662(7)	49(6)
C(6)	10561(8)	3390(7)	9945(7)	43(6)
C(7)	10332(10)	3972(7)	8709(8)	53(6)
C(8)	7206(8)	3606(8)	9842(7)	40(6)
C(9)	9680(8)	1770(8)	10664(7)	47(5)
C(10)	10086(9)	2911(8)	7798(7)	41(5)
C(11)	10410(8)	2340(7)	7330(7)	42(6)
C(12)	11278(9)	2191(8)	7265(7)	42(6)
C(13)	11847(10)	2642(9)	7661(8)	58(7)
C(14)	11536(9)	3219(8)	8129(7)	50(6)
C(15)	10654(10)	3352(8)	8213(7)	39(6)
C(16)	7049(7)	2915(7)	8598(7)	31(5)
C(17)	6760(8)	2885(8)	7848(7)	41(5)
C(18)	6395(9)	3495(8)	7485(7)	40(5)
C(19)	6303(8)	4176(8)	7916(7)	46(6)
C(20)	6575(8)	4210(8)	8663(8)	46(6)
C(21)	6944(8)	3574(8)	9021(8)	38(5)
C(22)	9040(9)	1008(7)	9614(7)	40(5)
C(23)	8523(9)	408(7)	9357(8)	42(5)
C(24)	8039(9)	−7(8)	9854(8)	42(6)
C(25)	8041(9)	201(7)	10621(9)	50(6)
C(26)	8558(10)	769(8)	10879(8)	50(6)
C(27)	9064(9)	1182(7)	10381(7)	35(5)
C(28)	11616(13)	1542(9)	6771(8)	70(8)
C(29)	12585(12)	1563(11)	6638(11)	159(13)
C(30)	11454(14)	851(9)	7166(10)	154(13)
C(31)	11164(13)	1543(9)	6010(9)	138(11)
C(32)	6062(12)	3461(10)	6680(8)	71(7)
C(33)	5090(13)	3227(13)	6747(10)	183(14)
C(34)	6499(15)	2870(10)	6228(8)	197(16)
C(35)	5968(16)	4183(9)	6288(9)	163(14)
C(36)	7457(11)	−688(8)	9599(9)	60(7)
C(37)	6531(11)	−549(10)	9790(10)	113(10)
C(38)	7767(10)	−1388(8)	9988(10)	105(9)
C(39)	7548(11)	−844(9)	8760(9)	104(10)
O(11)	3454(12)	664(9)	4828(9)	166(9)
C(40)	3927(19)	947(13)	4362(12)	120(12)
C(41)	4343(17)	528(11)	3771(12)	208(18)
C(42)	4101(14)	1739(11)	4434(11)	164(13)
O(12)	4546(9)	1081(8)	7668(7)	119(7)
C(43)	5113(13)	887(10)	7276(11)	68(9)
C(44)	5010(11)	887(9)	6412(9)	93(8)
C(45)	5999(11)	673(10)	7544(10)	120(10)

[a] Equivalent isotropic *U* defined as one-third of the trace of the orthogonalized $\mathbf{U}_{ij}$ tensor.

From a methanolic solution of Cr^{II}_2(acetate)$_4$, the ligand H_3L·3HCl, and NEt_3 were obtained light green crystals of [LCr^{III}] (**4**) upon slow diffusion of air into the solution. Reaction of the trihydrochloride, H_3L·3HCl, with manganese(III) acetate, [$Mn^{III}_3(\mu$-O)(μ-acetate)$_6$][acetate], and NEt_3 in methanol under strictly anaerobic conditions produced a yellow-brown crystalline precipitate of [LMn^{III}] (**5**). Its oxidized form [LMn^{IV}]PF_6 (**5a**) was obtained from the reaction of **5** with [Fc]PF_6 (1:1) in acetone as green microcrystals. The preparation of blue-green [LFe^{III}] was described previously.[14] [LCo] (**6**) was obtained as a gray powder from the above methanolic solution of the ligand, NEt_3, and $CoCl_2$·6H_2O. The neutral complexes **1**−**6** are insoluble in water but dissolve in acetonitrile, dichloromethane, chloroform, or dimethylformamide.

Chart 1. Complexes and Their Labeling

Mononuclear complexes

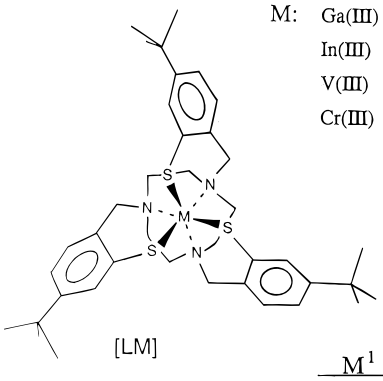

Dinuclear complexes

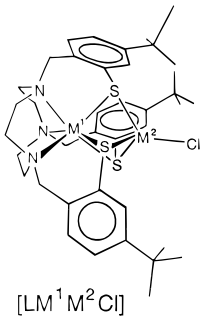

M^1	M^2	
Mn(II)	Mn(II)	**7**
Co(II)	Co(II)	**8**
Ni(II)	Ni(II)	**9**
Zn(II)	Zn(II)	**10**
Cd(II)	Cd(II)	**11**
Zn(II)	Fe(II)	**12**
Zn(II)	Co(II)	**13**
Zn(II)	Ni(II)	**14**
Ni(II)	Co(II)	**15**
Ni(II)	Zn(II)	**16**
Mn(II)	Fe(II)	**17**
Mn(II)	Co(II)	**18**
Mn(II)	Ni(II)	**19**
Mn(II)	Zn(II)	**20**
Mn(II)	Cd(II)	**21**
Mn(II)	Hg(II)	**22**

In the above section, we have described the preparation of mononuclear complexes [LM^{III}] from reaction mixtures containing L and M^{III} in a 1:1 ratio. Since the three monodentate thiophenolate groups are facially bound and electron rich, these mononuclear complexes may function as ligands for other metal ions. In this section, we shall first describe the preparation of a series of homodinuclear complexes of the type [LM_2Cl] where one metal ion is six-coordinate (N_3S_3 donor environment) whereas the second metal ion is four-coordinate (S_3Cl donor set). Thus the thiophenolate groups are now bridging two metal ions in a face-sharing octahedral/tetrahedral fashion. In the second part, we show that it is possible to selectively substitute the tetrahedrally coordinated metal ion by a different metal ion, generating thereby heterodinuclear complexes of the type [LM^1M^2Cl]. We adopt the following convention for this formula: the metal M written next to the ligand L is always six-coordinate ($N_3S_3M^1$) whereas the other metal M adjacent to the chloro ligand is always four-coordinate (S_3ClM^2). It is then immediately clear that, in principle, two linkage isomers exist for each heterodinuclear species: [LM^1M^2Cl] and [LM^2M^1-Cl].

The homodinuclear [LM_2Cl] complexes where (M = Mn^{II} (**7**), Co^{II} (**8**), Ni^{II} (**9**), Zn^{II} (**10**), and Cd^{II} (**11**) were prepared under anaerobic conditions as crystalline materials by the reaction of H_3L·3HCl in methanol with 2 equiv of the respective chloride salts MCl_2·6H_2O and excess tetraethylammonium chloride and triethylamine, eq 1. Excess [NEt_4]Cl is necessary to prevent excessive dissociation of the chloro ligand in the [LMMCl] products.

$$\mathrm{H_3L{\cdot}3HCl + 2MCl_2{\cdot}6H_2O \xrightarrow[CH_3OH]{Et_3N/[Et_4N]Cl} [LMMCl]} \quad (1)$$

The heterodinuclear complexes $[LM^1M^2Cl]$ were prepared by either of the two following procedures. In some cases, the stability of the $[LM^1]^-$ fragment is so large that the corresponding homodinuclear species $LM^1{}_2Cl$ reacts with a different metal dichloride with exchange of the tetrahedrally coordinated metal ion, eq 2a. Alternatively, the mononuclear monoanionic species

$$\mathrm{LM^1{}_2Cl + M^2Cl_2 \xrightarrow{-M^1Cl_2} [LM^1M^2Cl]} \quad (2a)$$

$[LM]^-$ was prepared *in situ* from $[LM_2Cl]$ by addition of 2 equiv of 1,4,7-triazacyclononane (tacn) in methanol, eq 2b. This

$$\mathrm{[LM^{II}{}_2Cl] + 2tacn \rightarrow [LM^{II}]^- + [M(tacn)_2]^{2+}} \quad (2b)$$

species reacts then with 1 equiv of $M^2Cl_2{\cdot}6H_2O$, yielding the heterodinuclear species $[LM^{II}M^2Cl]$, eq 3.

$$\mathrm{[LM^{II}]^- + M^2Cl_2{\cdot}6H_2O \xrightarrow[[Et_4N]Cl]{CH_3OH} [LM^{II}M^2Cl]} \quad (3)$$

The species $[LM^{II}]^-$ can also be obtained from a 1:1 reaction mixture of the ligand and M^{II}.

The heterodinuclear complexes prepared in this work are summarized and labeled in Chart 1; three series have been synthesized: (i) $[LZn^{II}M^2Cl]$ ($M^2 = Fe^{II}$ (**12**), Co^{II} (**13**), Ni^{II} (**14**), (ii) $[LNi^{II}M^2Cl]$ ($M^2 = Co^{II}$ (**15**), Zn^{II} (**16**), and (iii) $[LMn^{II}M^2Cl]$ ($M^2 = Fe^{II}$ (**17**), Co^{II} (**18**), Ni (**19**), Zn^{II} (**20**), Cd^{II} (**21**), Hg^{II} (**22**). Their chemical identity has been proven by elemental analysis and mass spectrometry. We have been able to show that metal ion scrambling as in eq 4 does not occur under the reaction conditions used here. This was achieved by

$$\mathrm{[LM^1M^2Cl] \not\rightleftharpoons [LM^2M^1Cl]} \quad (4)$$

fast atom bombardment (FAB) mass spectrometry. The results are given in Table S1. The mononuclear species show the molecular ion peak $[LM]^+$ as the most intense peak and two intense fragment ion peaks: $[LM - 1\,(C_{11}H_{14}S)]^+$, $[LM - 2(C_{11}H_{14}S)]^+$ ($C_{11}H_{14}S$ is one pendant arm of the macrocycle L). These peaks are also clearly detected in the spectra of the dinuclear species where their actual *m*/*z* values and the isotopic distribution patterns are dependent on the nature of the six-coordinated metal ion. Thus, for the linkage isomers **14** and **16** the molecular ion peak $[LM^1M^2Cl]^+$ is observed at $m/z = 819$ for both complexes but the $[LM^1]^+$ fragment peaks are found at *m*/*z* 724.2 for **14** ($[LZn]^+$) and at *m*/*z* 718.3 for **16** ($[LNi]^+$). In addition, all dinuclear complexes exhibit an intense peak for the $[LM^1M^2]^+$ fragment which is, of course, the same for the two linkage isomers **14** and **16**.

All complexes of the type $[LM^1M^2Cl]$ are soluble in acetone. From such solutions excellent-quality crystalline materials of $[LM^1M^2Cl]$2 acetone can be obtained. The crystals lose these acetone molecules of crystallization upon storage in air at ambient temperature within a few hours or days.

^{1}H NMR Spectra. Table 4 gives chemical shifts and assignments of the 400 MHz ^{1}H NMR spectra of **2**, **10**, and **11** in $CDCl_3$ according to the labeling in Chart 2. Complex **2** possesses C_3 symmetry, and consequently, there are 10 chemically distinct protons. The protons of the $N-CH_2-CH_2-N$ moiety (protons f, g, h, i) of the 1,4,7-triazacyclononane backbone of L show a complicated multiplet which was assigned in accordance with the analysis reported for $[Ti^{IV}(tapt)]^+$,[5] where tapt represents 1,4,7-tris(5-*tert*-butyl-2-hydroxybenzyl)-1,4,7-triazacyclononane, which is a tris(phenolate) analog of L. The

Table 4. 400 MHz ^{1}H NMR Data for **2**, **10**, and **11** in $CDCl_3$

δ, ppm[a] **2**	**10**	**11**	integration	assignt[b]	δ, ppm[a] **2**	**10**	**11**	integration	assignt[b]
7.40	7.83	7.57	3H	a	3.17	3.36	3.20	3H	f
6.86	7.00	6.99	3H	b	2.80	3.19	3.17	3H	g
6.85	6.92	6.90	3H	c	2.58	2.65	2.11	3H	h
4.92	4.23	4.25	3H	d	2.31	2.32	2.28	3H	i
3.35	3.33	3.35	3H	e	1.25	1.33	1.33	27H	j

coupling const	value[c] **2**	**10**	**11**	coupling const	value[c] **2**	**10**	**11**
J_{fg}	15	13	*d*	J_{fh}	13	15	*d*
J_{hi}	13	15	*d*	J_{ab}	2	2	1.5
J_{fi}	4	4	*d*	J_{bc}	8	8	7.8
J_{gh}	5	5	*d*	J_{de}	12	12	11.5
J_{gi}	0	0	0				

[a] Chemical shift. [b] See Chart 2 for proton labels. [c] Coupling constants in Hz. [d] Due to overlap of resonances not determined.

Chart 2. ^{1}H NMR Labeling Scheme

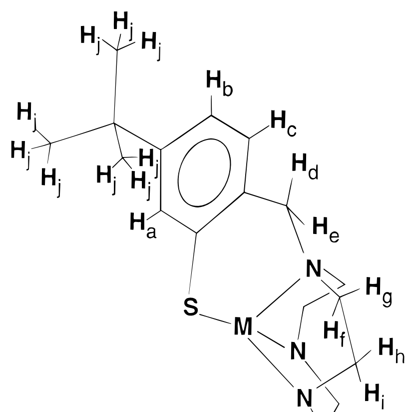

fact that no coupling between protons g and i is observed allows the conclusion that the dihedral angle between the planes defined by H_i-C-C and H_g-C-C is 80–90°.

The ^{1}H NMR spectra of **2**, **10**, and **11** clearly show that, even at room temperature, the conformation of the three five-membered chelate rings M–N–C–C–N is rigidly fixed in solution. No evidence for fluctional behavior was detected.[11,12] Since C_3 symmetry prevails, the coordinated 1,4,7-triazacyclononane backbone adopts a $(\lambda\lambda\lambda)_5$ or $(\delta\delta\delta)_5$ conformation, where the subscript denotes the fact that the three chelate rings, M–N–C–C–N, are five-membered in contrast to the pendant arm chelates, M–N–C–C=C–S, which are six-membered.

The homodinuclear complexes **10** and **11** also possess C_3 symmetry, and their ^{1}H NMR spectra are very similar, indicating stereochemical rigidity of the coordinated ligand in solution at ambient temperature.

Crystal Structures. Table 5 summarizes selected bond distances and angles of $[LCo^{III}]$, **6**, and of the dinuclear complex [LZnNiCl], **14**.

The quality of the crystal structure determination of **6** is rather low because of low diffraction power of the crystal at higher 2θ values, but it does confirm the atom connectivity. Crystals of **6** consist of mononuclear neutral LCo^{III} molecules as shown in Figure 1. Complex **6** is isostructural with $[LFe^{III}]$.[14] The cobalt(III) ion is facially coordinated to three amine nitrogen atoms of the 1,4,7-triazacyclononane backbone of L^{3-} and three thiophenolato sulfur donor atoms. The average Co–N bond distance at 2.04(3) Å is rather long in comparison to the analogous bonds in $[Co(tacn)(ttcn)]^{3+}$ at 1.96(1) Å[21] (tacn = 1,4,7-triazacyclononane, ttcn = 1,4,7-trithiacyclononane) whereas

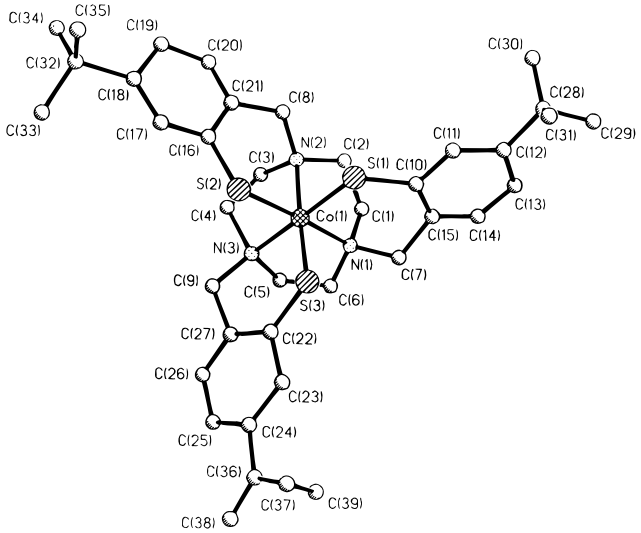

Figure 1. Schematic representation of the neutral molecule in crystals of **6**.

Table 5. Selected Bond Distances (Å) and Angles (deg)

	Complex **6**		
Co1−S1	2.25(1)	Co1−S2	2.24(1)
Co1−S3	2.23(1)	Co1−N1	2.03(3)
Co1−N2	2.08(3)	Co1−N3	2.00(5)
S1−C10	1.72(5)	S2−C16	1.73(4)
S3−C22	1.68(4)		
S1−Co1−S2	84.5(5)	S1−Co1−S3	83(1)
S2−Co1−S3	84.6(5)	S1−Co1−N1	98(1)
S2−Co1−N1	176.9(10)	S3−Co1−N1	94(1)
S1−Co1−N2	93.0(1)	S2−Co1−N2	94(1)
S3−Co1−N2	176.0(1)	N1−Co1−N2	87(1)
S1−Co1−N3	175.0(1)	S2−Co1−N3	91(1)
S3−Co1−N3	94.0(1)	N1−Co1−N3	86(2)
N2−Co1−N3	90.0(2)	Co1−S1−C10	111(2)
Co1−S2−C16	113.0(2)	Co1−S3−C22	114(1)
	Complex **14**		
Ni1−S1	2.325(4)	Ni1−S2	2.333(4)
Ni1−S3	2.331(4)	Ni1−Cl1	2.197(5)
Ni1···Zn1	2.956(2)	S1−Zn1	2.583(4)
S1−C10	1.78(1)	S2−Zn1	2.564(4)
S2−C16	1.78(1)	S3−Zn1	2.578(4)
S3−C22	1.78(1)	Zn1−N1	2.22(1)
Zn1−N2	2.25(1)	Zn1−N3	2.21(1)
S(1)−Ni(1)−S(2)	92.1(1)	S(1)−Ni(1)−S(3)	93.8(1)
S(2)−Ni(1)−S(3)	92.9(1)	S(1)−Ni(1)−Cl(1)	123.2(2)
S(2)−Ni(1)−Cl(1)	127.0(2)	S(3)−Ni(1)−Cl(1)	119.1(2)
Ni(1)−S(1)−Zn(1)	73.8(1)	Cl(1)−Ni(1)−Zn(1)	175.6(2)
Zn(1)−S(1)−C(10)	94.1(4)	Ni(1)−S(1)−C(10)	99.0(5)
Ni(1)−S(2)−C(16)	101.3(4)	Ni(1)−S(2)−Zn(1)	74.1(1)
Ni(1)−S(3)−Zn(1)	73.9(1)	Zn(1)−S(2)−C(16)	94.1(4)
Zn(1)−S(3)−C(22)	93.8(4)	Ni(1)−S(3)−C(22)	99.4(5)
S(2)−Zn(1)−S(3)	82.2(1)	S(1)−Zn(1)−S(2)	81.3(1)
S(1)−Zn(1)−N(1)	87.6(3)	S(1)−Zn(1)−S(3)	82.4(1)
S(3)−Zn(1)−N(1)	112.8(3)	Ni(1)−Zn(1)−N(1)	130.8(3)
S(1)−Zn(1)−N(2)	113.3(3)	S(2)−Zn(1)−N(1)	160.1(3)
S(3)−Zn(1)−N(2)	160.2(3)	Ni(1)−Zn(1)−N(2)	132.3(3)
Ni(1)−Zn(1)−N(3)	131.8(3)	S(2)−Zn(1)−N(2)	88.2(3)
S(2)−Zn(1)−N(3)	113.3(3)	N(1)−Zn(1)−N(2)	81.1(4)
N(1)−Zn(1)−N(3)	81.3(4)	S(1)−Zn(1)−N(3)	161.5(3)
		S(3)−Zn(1)−N(3)	88.2(3)
		N(2)−Zn(1)−N(3)	79.7(4)

the average Co−S bond at 2.24(1) Å is very similar to those found in $[Co(tacn)(ttcn)]^{3+}$, $[Co(tasn)_2]^{3+}$,[22] $[Co(en)_2(S_2CH_2CH_2NH_2)]^{2+}$,[23] and $[Co(en)_2(SCH_2CO_2)]^{+}$,[23] regardless whether the sulfur donor atom stems from a mercapto or thioether ligand. Interestingly, the average S−Co−S angle of 84° is significantly smaller than 90°. For three strong π-donating ligands in *cis* positions relative to each other, this angle is expected to be >90°. This is taken as an indication that the R−S$^-$ groups in **6** are weak π-donors.

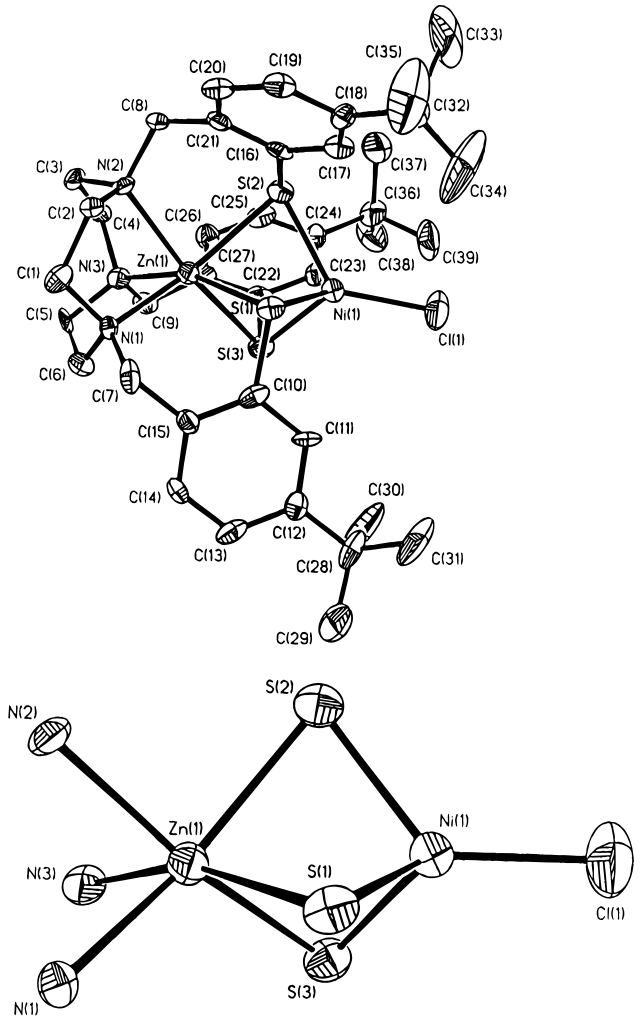

Figure 2. Structure of the neutral molecule in crystals of **14**·2(acetone) (top) and of the first coordination spheres of the metal ions (bottom).

Red-orange single crystals of [LZnNiCl]·2(acetone), **14**, suitable for X-ray crystallography were obtained from an acetone solution by slow evaporation of the solvent. Figure 2 shows the structure of a neutral molecule. The zinc ion is six-coordinate in an N_3S_3 donor set intermediate between octahedral and trigonal prismatic geometry. The twist angle Θ defined as follows, is 35°; it is 60° in a regular octahedron and 0° in a trigonal prism.

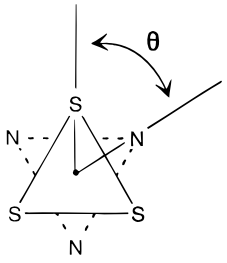

The nickel ion is four-coordinate in a three thiophenolate sulfur and one coordinated chloride ligand environment with

(21) Küppers, H.-J.; Wieghardt, K.; Steenken, S.; Nuber, B.; Weiss, J. *Z. Anorg. Allg. Chem.* **1989**, *573*, 43.
(22) Hambley, T. W.; Gahan, L. R. *Acta Crystallogr.* **1986**, *C42*, 1322.
(23) Elder, R. C.; Florian, L. R.; Lake, R. E.; Yacynych, A. M. *Inorg. Chem.* **1973**, *12*, 2690.
(24) Silver, A.; Millar, M. *J. Chem. Soc., Chem. Commun.* **1992**, 948.

Table 6. Electronic Spectral Data for Complexes **1**−**22**[a]

complex	λ_{max}, nm (ϵ, L mol^{-1} cm^{-1})	solvent	μ_{eff}, μ_B (293 K)
1	278 (3.8×10^4)	$CHCl_3$	dia
2	278 (4.2×10^4)	$CHCl_3$	dia
3	250 (2.6×10^4), 280 (1.6×10^4), 346 (1.2×10^4), 491 (3.0×10^3), 566 (3.0×10^3)	CH_3CN	2.84
3a	483 sh (7.0×10^3), 530 (6.9×10^3), 681 (6.8×10^3)	CH_3CN	1.94
3b	400 (4×10^3), 550 sh, 685 (2.0×10^4)	CH_3CN	
4	357 (13.3×10^3), 410 (6.2×10^3), 460 (390), 591 (290)	$CHCl_3$	3.85
5	280 (1.5×10^4), 356 (8.8×10^3), 434 (7.6×10^3), 737 (780)	$CHCl_3$	5.04
5a	378 (9.8×10^3), 667 (5.5×10^3)	$CHCl_3$	4.5
6	316 (4.5×10^4), 430 sh, 523 (480), 652 (460), 1060 (5)	$CHCl_3$	dia
7	not measd		4.9
8	280 (2.2×10^4), 313 (2.4×10^4), 596 (474), 615 (473), 745 (382), 1523 (186)	$CHCl_3$	5.62
9	455 (2.1×10^3), 510 (1.3×10^3), 595 (850), 650 sh (560), 730 sh (320), 997 (142), 1150 (115)	$CHCl_3$	2.6
10	275 (2.4×10^4)	$CHCl_3$	dia
11	253 (2.8×10^4), 297 (2.4×10^4)	CH_2Cl_2	dia
12	not measd		5.4
13	268 (1.8×10^4), 350 sh (3.0×10^3), 410 (1.8×10^3), 590 (450), 630 (600), 750 (540), 1570 (200)	$CHCl_3$	4.5
14	280 (1.8×10^4), 350 (4.8×10^3), 460 (2.1×10^3), 510 (2.0×10^3), 702 (133), 1005 (61), 1152 (46), 1275 (30), 1540 (24)	$CHCl_3$	3.2
15	280 (1.6×10^4), 400 sh (3.0×10^3), 596 (474), 615 (473), 745 (382), 1062 (77), 1523 (186)	$CHCl_3$	5.4
16	280 (1.3×10^4), 360 (3.9×10^3), 400 (2.5×10^3), 657 (53), 1000 sh, 1140 (60)	$CHCl_3$	3.1
17	360 sh, 422 (2.1×10^3)	$CHCl_3$	5.8
18	279 (1.6×10^4), 440 sh, 465 (1.2×10^3), 596 sh, 623 (730), 771 (450), 1510 (210)	$CHCl_3$	4.9
19	328 sh, 410 (2.7×10^3), 446 (1.7×10^3), 485 sh, 646 (740), 755 sh, 1023 (52), 1260 (40)	$CHCl_3$	5.0
20	767	refl	5.8
21	360 sh, 436 (470), 635 (15), 730 sh, 771 (23), 865 (19)	$CHCl_3$	5.9
22	not measd		5.9
$[LNi]^-$	610 (63), 930 (65), 1050 sh (54)	CH_3OH	

[a] Abbreviations: dia = diamagnetic; refl = reflectance spectrum.

idealized C_{3v} symmetry of the S_3NiCl polyhedron. Thus, all three thiophenolate groups of L form μ_2-S bridges in a face-sharing fashion.

The average Ni−S bond distance at 2.33(1) Å is rather long as compared with those of the bridging thiolates in [(RS)Ni(μ-SR)$_3$Ni(SR)][24] (Ni−S 2.267(3)−2.324(3) Å). The Ni−Cl bond at 2.197(5) Å is quite short; it is 2.27(1) Å in $[Ph_3MeAs]_2[NiCl_4]$.[25] The Zn−S bonds in **14** are rather long even for bridging thiolates (average 2.575(4) Å) whereas the Zn−N distances are in the normal range observed for octahedral zinc(II) complexes with a coordinated 1,4,7-triazacyclononane ligand.[26] The Ni···Zn distance is 2.956(2) Å and should be compared with a Ni···Ni distance of 2.607(3) Å in [(RS)Ni(μ-SR)$_3$Ni(SR)],[24] which contains two face-sharing tetrahedral Ni(II) ions.

Electronic Spectra. Table 6 summarizes electronic solution spectral data and effective magnetic moments at 293 K of the complexes.

Because of the presence of three S-coordinated thiophenolate groups, the electronic spectra are dominated by intense, spin-allowed ligand charge transfer (CT) transitions. Mono- and dinuclear complexes containing metal ions with a d^0 or d^{10} electron configuration like **1**, **2**, and **10** display one intense absorption maximum in the 260−300 nm range which is assigned to a $\pi \rightarrow \pi^*$ transition of the thiophenolates. In addition, in some cases (**3**, **11**) a second such transition at higher energy is observed (∼250 nm). One or both of these bands are observed in all spectra recorded irrespective of the nature of the coordinated metal ion.

The spectra of most mononuclear complexes containing a tri- or tetravalent transition metal ion with a 3 d^n electron configuration with $n < 6$ display two or more very intense ($\epsilon > 1000$ L mol^{-1} cm^{-1}) absorption maxima in the visible region (>350 nm) which are assigned to thiophenolate-to-metal CT transitions (Figures S1 and S2 (Supporting Information)). Interestingly, the spectrum of [LCo^{III}], **6**, with a low-spin t_{2g}^6 configuration exhibits three low-intensity transitions in the visible region at 523, 652, and 1060 nm which are assigned to d−d transitions, the first two of which are probably $^1A_{1g} \rightarrow {}^1T_{2g}$ (ν_2) and $^1A_{1g} \rightarrow {}^1T_{1g}$ (ν_1) in O_h symmetry which gain intensity because the symmetry of the N_3S_3Co polyhedron is C_3. The very weak band at 1065 nm is tentatively assigned to a spin-forbidden $^1A_{1g} \rightarrow {}^3T_{2g}$ transition. If these assignments are correct, one can calculate the ligand field parameters Dq and B to be 1630 cm^{-1} and 236 cm^{-1}, respectively. The low value for B is in good agreement with the notion that the Co−S bond has a significant degree of covalency. For the corresponding tris(phenolato)cobalt(III) complex [Co(tapt)][5] $Dq = 2000$ cm^{-1} and $B = 545$ cm^{-1}. For comparison, a few values of Dq and B are listed for some octahedral cobalt(III) complexes in Table S2 (Supporting Information). From these values it follows that the tris(thiophenolato) ligand L^{3-} induces a significantly weaker ligand field than its tris(phenolate) analog.

If the two low-energy and low-intensity maxima at 460 and 591 nm in the spectrum of [LCr^{III}], **4** (Figure S2), are assigned to $^4A_2 \rightarrow {}^4T_1(F)$ (ν_2) and $^4T_2(F) \leftarrow {}^4A_2(F)$ (ν_1) d−d transitions, values for Dq and B of 1690 cm^{-1} and 445 cm^{-1}, respectively, can be calculated from the relation $\nu_1 = 10Dq$ (in O_h symmetry for simplicity). Again, a low value for B indicates considerable covalency of the Cr−S bond; in comparison, B is 620 cm^{-1} for $[Cr(tacn)_2]^{3+}$ containing the pure σ-donor ligand 1,4,7-triazacyclononane (Table S2). For the corresponding tris(phenolato) complex [Cr(tapt)][5] Dq is found to be 1760 cm^{-1} and $B = 533$ cm^{-1}, which represents again a stronger ligand field than in **4**. The spectrum of [LMn^{III}], **5** (Figure S2), displays a low-intensity d−d transition at 737 nm which is assigned to $^5E_g \rightarrow {}^5T_{2g}$ (in O_h symmetry), yielding a value for Dq of 1357 cm^{-1}.

The complex $[LNi^{II}]^-$ was generated *in situ* in methanol solution from [LNiZnCl] or [LNiNiCl] by addition of 2 equiv of 1,4,7-triazacyclononane, yielding 1 equiv of $[M(tacn)_2]^{2+}$ and $[LNi]^-$, respectively. The electronic spectrum (Table 6) displays two typical d−d transitions in the visible region for octahedral

(25) Pauling, P. *Inorg. Chem.* **1966**, *5*, 1498.
(26) Chaudhuri, P.; Stockheim, C.; Wieghardt, K.; Deck, W.; Gregorzik, R.; Vahrenkamp, H.; Nuber, B.; Weiss, J. *Inorg. Chem.* **1992**, *31*, 1451.

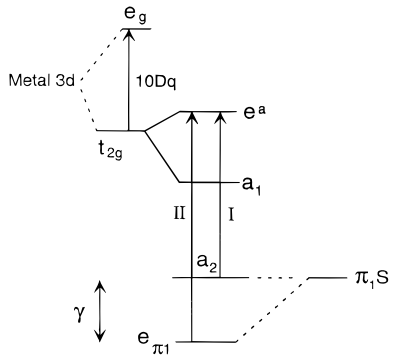

Figure 3. Simplified one-electron molecular orbital energy level diagram for [LM^{III}] complexes. The lowest energy observed charge-transfer transitions are shown by arrows. The scheme is adapted from Figure 7 in ref 27.

Ni(II) which allows estimates of $Dq = 1010$ cm^{-1} and $B = 920$ cm^{-1}. This implies a ligand field strength of [LNi]$^-$ similar to that of $[Ni(OH_2)_6]^{2+}$ ($Dq = 890$ cm^{-1}, $B = 905$ cm^{-1}) and much smaller than that of $[Ni(tacn)_2]^{2+}$ ($Dq = 1235$ cm^{-1}, $B = 980$ cm^{-1}). Since Ni−S π-bonding is considered to be small because the metal t_{2g} orbitals are filled, this represents a measure of the σ-donor properties of L^{3-}.

The electronic spectra of [LV^{III}] (**3**), [LV^{IV}]$^+$ (**3a**), and [LV^{V}]$^{2+}$ (generated electrochemically only), shown in Figure S1, and of [LMn^{IV}]$^+$ (Figure S2) and high-spin [LFe^{III}][14] are dominated by at least two intense ($\epsilon > 10^3$ L mol^{-1} cm^{-1}) thiophenolate-to-metal CT bands in the visible region (Table 6). In the following qualitative analysis of these spectra, we follow closely the analysis of the CT bands of tris(catecholato)-iron(III) complexes reported by Solomon, Raymond, et al.,[27] who have assigned the CT band II at higher energy and the lower energy band I (see Figure 3) to transitions from the catecholate oxygen donor (the ligand $e_{\pi 1}$ orbitals are stabilized relative to the a_2 ligand orbital upon complexation) to the metal orbitals. The t_{2g} metal orbitals split in D_3 symmetry into an e^a and a_1 set. Single-crystal polarized absorption and magnetic circular dichroism spectroscopy on these tris(catecholate)iron-(III) complexes has then shown that the two *x*,*y*-polarized transitions in the visible region are $e_{\pi 1} \rightarrow e^a$ (II) and $a_2 \rightarrow e^a$ (I) CT transitions (Figure 3). The energy difference γ(II−I) thus is a direct measure of the amount of π-bonding because the "a_2 ligand orbital has no metal orbital of the same symmetry close enough in energy to stabilize it significantly and is therefore virtually nonbonding".[27] If the same is true for the C_3 symmetric tris(thiophenolato)metal complexes described here, one can calculate this energy difference γ to be 2460 cm^{-1} for [LFe^{III}], which is significantly smaller than those reported for the corresponding tris(catecholato)iron(III) complexes ($\gamma = 3500-4300$ cm^{-1}) and 2700 cm^{-1} for [LV^{III}]. This would again agree with the notion that thiophenolates have lesser π-donating capabilities than catecholates or phenolates.

In the following, we describe the electronic solution spectra of [LM^{1}M^{2}Cl] complexes which contain divalent transition metal ions in an octahedral/prismatic N_3S_3 and a tetrahedral S_3Cl ligand environment.

The homodinuclear complexes **10** and **11** contain d^{10} Zn(II) and Cd(II) ions, and consequently, only very intense ligand $\pi \rightarrow \pi^*$ transitions in the ultraviolet region are observed (Table 6). The two heterodinuclear linkage isomers, namely red [LZnNiCl], **14**, and green [LNiZnCl], **16**, therefore allow an investigation of the spectral features of an "octahedral" Ni(II) in **16** and a "tetrahedral" one in **14** without interference of bands arising from the zinc(II) metal ion in the visible region. The two spectra are shown in Figure S3 (Supporting Information). For **14**, five weak d−d transitions >700 nm are observed, which is typical for a "tetrahedral" nickel(II) in idealized C_{3v} symmetry.[28,29] In contrast, the spectrum of **16** displays only two weak d−d transitions at 1140 and 657 nm, where the former is asymmetric. From this, rough estimates of *Dq* and *B* can be obtained for **16** of 939 cm^{-1} and 853 cm^{-1}, respectively. These values can be compared with those reported for $[Ni(H_2O)_6]^{2+}$ ($Dq = 890$ and $B = 905$ cm^{-1}) and $[Ni(tacn)_2]^{2+}$ [30] ($Dq = 1235$, $B = 980$ cm^{-1}). As noted above, the ligand field of this N_3S_3 donor set is comparable to that of H_2O. It is interesting to note that binding of the [LNi]$^-$ complex to the ZnCl fragment in **16** lowers the ligand field strength and the Racah parameter somewhat. Thus, the covalency of the Ni−S bond (π-bonding) is increased in **16** whereas its σ-donor strength is lower in **16** than in [LNi]$^-$. The spectrum of [LNi$_2$Cl], **9**, is not a simple superposition of the spectra of [LNi]$^-$ and [LZnNiCl] or **14** and **16**. As described below, the two nickel(II) ions in **9** are strongly antiferromagnetically coupled, which leads to a drastic change in the spectral properties of the individual ion.

"Tetrahedral" Co(II) is readily detected in the spectra of complexes **8**, **13**, **15**, and **18** because the intensity of the d−d transitions of Co(II) is generally much larger for tetrahedral than for octahedral complexes. Figure S4 (Supporting Information) shows the spectra of [LZnCoCl] (**13**) and [LMnCoCl] (**18**). For tetrahedral Co(II), the following spin-allowed d−d transitions in T_d symmetry are expected: $^4A_2(F) \rightarrow {}^4T_1(P)$ (ν_3), $^4A_2(F) \rightarrow {}^4T_2(F)$ (ν_2), and $^4A_2(F) \rightarrow {}^4T_1(F)$. The maximum at ∼1500 nm is assigned to ν_2,[31] whereas ν_3 is split (C_{3v} symmetry) into two maxima at ∼620 and 770 nm for all complexes. By using the relations[32] $\nu_2 = 1.5Dq + 7.5B' - Q$ and $\nu_3 = 1.5Dq + 7.5B' + Q$, where $Q = {}^1/_2\,[(0.6\Delta - 15B')^2 + 0.64\Delta^2]^{1/2}$, we obtain values for *Dq* and *B* of 384 cm^{-1} and 751 cm^{-1}, respectively, for complex **18**. The values of *Dq* are 380 cm^{-1} for **15**, 368 cm^{-1} for **13**, and 384 cm^{-1} for **8**, whereas *B* values are calculated to be 700 cm^{-1} for **15**, 710 cm^{-1} for **13**, and 700 cm^{-1} for **8**. These values are quite typical for tetrahedral Co-(II) complexes.

Magnetic Properties of Complexes. Temperature-dependent molar magnetic susceptibilities for powdered samples of complexes were measured on a Faraday balance in the range 80−293 K or in some instances on a SQUID magnetometer in the range 2−300 K. The effective magnetic moments, μ_{eff}, at 293 K are summarized in Table 6.

The mononuclear species **3**, **3a**, **4**, **5**, and **5a** display nearly temperature-independent magnetic moments (80−293 K) typical for octahedral complexes with d^2, d^1, d^3, and d^4 high spin and d^3 electron configurations, respectively. For solid [LFe^{III}], with a d^5 electron configuration, a temperature-dependent high-spin−low-spin crossover equilibrium has been reported,[14] but in solution at 293 K the high-spin form prevails.

The dinuclear complexes **12**, **13**, **14**, **16**, **20**, **21**, and **22** each contain one paramagnetic and one diamagnetic metal ion. Complexes **20**−**22** contain a high-spin d^5 six-coordinate Mn-(II) ion, and consequently, a temperature-independent μ_{eff} of 5.9 μ_B is observed for each compound. Complexes **12**−**14** contain tetrahedral Fe^{II}(d^6), Co^{II}(d^7), and Ni^{II}(d^8) metal ions,

(27) Karpishin, T. B.; Gebhard, M. S.; Solomon, E. I.; Raymond, K. N. *J. Am. Chem. Soc.* **1991**, *113*, 2977.
(28) Bertini, I.; Gatteschi, D.; Mani, F. *Inorg. Chem.* **1972**, *11*, 2464.
(29) Gerloch, M.; Manning, M. R. *Inorg. Chem.* **1981**, *20*, 1051.
(30) Hart, S. M.; Boeyens, J. C. A.; Hancock, R. D. *Inorg. Chem.* **1983**, *22*, 982.
(31) Lever, A. B. P. *Inorganic Electronic Spectroscopy*, 2nd ed.; Elsevier: Amsterdam, 1968.
(32) Cotton, F. A.; Goodgame, M. *J. Am. Chem. Soc.* **1961**, *83*, 1777.

Table 7. Magnetic Properties of Dinuclear Complexes [LM^1M^2Cl]

complex	M^1_{oct}	M^2_{tet}	g_1(oct)	g_2(tet)	J, cm^{-1} [a]	TIP, emu
7	Mn^{II}	Mn^{II}	1.98 (fixed)	1.9	−29	
8	Co^{II}	Co^{II}	2.1	2.1	−5	300×10^{-6}
15	Ni^{II}	Co^{II}	2.3	2.3	−9	300×10^{-6}
17	Mn^{II}	Fe^{II}	1.98 (fixed)	2.24	−24	

[a] $H = -2JS_1 \cdot S_2$; exchange coupling constant J from susceptibility measurements in the temperature range 80−293 K.

respectively, and a diamagnetic Zn^{II} ion. For **12** a temperature-independent μ_{eff} of 5.4 μ_B is typical for tetrahedral iron(II), whereas in **13** the magnetic moment varies from 4.5 μ_B at 293 K to 4.19 μ_B at 80 K, which is indicative of tetrahedral cobalt(II) ($S = {}^3/_2$).

For complex **14**, containing a tetrahedral $Ni^{II}(d^8)$, and for **16**, with an octahedral Ni^{II}, we have studied the temperature dependence of μ_{eff} in the range 2−300 K (Figure S5 (Supporting Information)). In agreement with the near-tetrahedral stereochemistry of the Ni(II) ion in **14**, the magnetic moment is strongly temperature dependent.[33] It decreases monotonically from 4.2 μ_B at 290 K to 3.2 μ_B at 40 K and then drops markedly to 1.1 μ_B at 2 K. In contrast, μ_{eff} of **16** is temperature independent at 3.1 μ_B in ×he range 290−10 K and then drops because of zero-field splitting to 2.2 μ_B at 2 K. The fit in Figure S5 was obtained with a g value of 2.2 and a zero-field-splitting parameter $|D|$ of 4.9 cm^{-1}.

The magnetic moment μ_{eff} at 293 K for the homo- and heterodinuclear complexes containing two paramagnetic metal ions per molecule (**7**−**9**, **15**, **17**−**19**) is always significantly smaller at ambient temperature than would be expected for two uncoupled ions ($\mu_{eff} = (\mu_1^2 + \mu_2^2)^{1/2}$). This indicates some degree of intramolecular antiferromagnetic coupling between the two ions. In three instances we have measured the temperature dependence in the range 2−290 K (complexes **9**, **18**, and **19**), and in all other cases the temperature range was 80−293 K.

In the latter cases the susceptibility data were satisfactorily fitted to the isotropic Heisenberg−Dirac−van Vleck model using the Hamiltonian $H = -2JS_1 \cdot S_2$ where J, g_1, and g_2 were treated as the only variables. Zero-field splitting and possible impurities of the samples were not taken into account. Although the resulting numerical values for J and, especially, g_1 and g_2 may not be very accurate, we can safely conclude that intramolecular antiferromagnetic coupling prevails, as the data in Table 7 show.

Magnetic susceptibility data for polycrystalline samples of **9**, **18**, and **19** were collected on a SQUID magnetometer in the temperature range 2−290 K in an external magnetic field of 1.0 T. The temperature dependence of the magnetic moment, μ_{eff}, of **9** is displayed in Figure 4; that of **18** and **19**, in Figure S6 (Supporting Information)).

The magnetic moment for [LNi_2Cl], **9**, decreases with decreasing temperature and approaches the value 0.35 μ_B/dinuclear unit at 2 K. This behavior is typical of antiferromagnetically coupled dinuclear paramagnetic centers ($S_1 = S_2 = 1$) with a diamagnetic ground state. A full-matrix diagonalization approach including exchange coupling ($-2JS_1 \cdot S_2$), Zeeman interactions, and an axial zero-field interaction (DS^2) was employed to fit the data. The least-squares fitting for **9**, shown as the solid line in Figure 4, of the experimental data leads to $J = -135$ cm^{-1}, $g_{oct} = 2.2$ (fixed), $g_{tet} = 2.2$ (fixed), $D_{oct} = 5$ cm^{-1}, $D_{tet} = 7$ cm^{-1} (fixed), and $E/D = 0$ (fixed). A temperature-independent paramagnetism (TIP) of 683×10^{-6} emu and a paramagnetic impurity ($S = 1$) of 2.2% were also included.

(33) Figgis, B. N.; Lewis, J. *Prog. Inorg. Chem.* **1964**, *6*, 37.

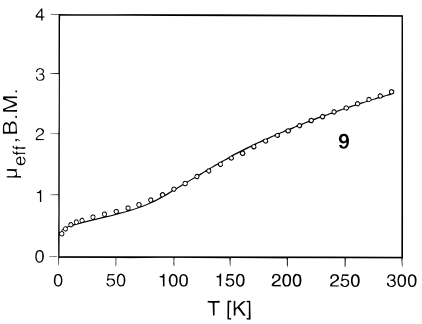

Figure 4. Temperature dependence of the magnetic moment, μ_{eff}, of **9**. The solid line represents a best fit of the data (see text); circles are experimental data.

Table 8. Electrochemistry of the Complexes[a]

complex	E,[b] V vs Ag/AgCl	solvent
1	1.08 ir, −0.70 ir	$CHCl_3$
3, **3a**	0.90 r, 0.19 r, −1.31 r	CH_3CN
4	0.65 ir	CH_2Cl_2
5, **5a**	0.10 r, −0.18 r	CH_3CN
[LFe^{III}][c]	1.02 ir; 0.24 r, −0.58 r	CH_2Cl_2
6	0.55 qr	CH_2Cl_2
[LNi]$^-$	0.18 ir, −0.13 qr	CH_3CN

[a] Cyclic voltammetry at 22 °C: 0.10 M tetra-*n*-butylammonium hexafluorophosphate supporting electrolyte; ∼10^{-5} M ferrocene internal standard; reference electrode Ag/AgCl (saturated LiCl in C_2H_5OH); glassy carbon working electrode; scan rate 100 mV s^{-1}; r = reversible; ir = irreversible; qr = quasi-reversible. [b] Potentials for reversible and quasi-reversible processes are midpotentials $E_{1/2} = (E_p^{ox} + E_p^{red})/2$ whereas for irreversible processes the peak potentials E_p^{ox} (or E_p^{red}) are given. All listed potentials were obtained from cyclic voltammograms recorded at a scan rate of 100 mV s^{-1}. [c] Reference 14.

The magnetic moment of [$LMn^{II}Co^{II}Cl$], **18**, decreases monotonically with decreasing temperature until it reaches a plateau at ∼50 K of 3.0 μ_B and drops below 20 K to 2.4 μ_B at 2 K. Thus, **18** possesses an $S_t = 1$ ground state, which is obtained via antiferromagnetic coupling between a high-spin Mn^{II} ($S = {}^5/_2$) and a cobalt(II) ion ($S = {}^3/_2$).

A fitting procedure as described above for **9** yields the solid line shown in Figure S6 with the following parameters: $J = -57$ cm^{-1}, $g_{Mn} = 2.0$ (fixed), $g_{Co} = 2.48$, $D_{Mn} = 3.0$ cm^{-1} (fixed), $D_{Co} = 10$ cm^{-1} (fixed), $E/D = 0$ (fixed), TIP = 400×10^{-6} emu; paramagnetic impurity ($S = {}^5/_2$) 9%.

Very similar magnetic behavior is observed for [LMnNiCl], **19**. Again μ_{eff} decreases with decreasing temperature to a plateau at ∼70 K (3.8 μ_B), which indicates an $S_t = {}^3/_2$ ground state. The best fit of the data yields the following parameters: $J = -49$ cm^{-1}, $g_{Mn} = 2.0$ (fixed), $g_{Ni} = 2.17$ (fixed), $D_{Mn} = 3.7$ cm^{-1}, $D_{Ni} = 7.0$ cm^{-1} (fixed), $E/D = 0$ (fixed), TIP = 600×10^{-6} emu (Figure S6).

Electrochemistry. Table 8 summarizes electrochemical data for the mononuclear complexes. Cyclic voltammograms (CV's) of acetonitrile, chloroform, or dichloromethane solutions containing 0.10 M tetra-*n*-butylammonium hexafluorophosphate as supporting electrolyte and ≈10^{-5} M complex were recorded with scan rates of 20−200 mV s^{-1}.

The CV's of **1** and **4** shown in Figures S7 (Supporting Information) each display one irreversible oxidation process at 1.08 and 0.65 V *vs* Ag/AgCl and a less developed irreversible reduction process at −0.70 and ∼−0.6 V, respectively. The latter process is only observed if the oxidative step is scanned prior to the reduction. In addition, **4** shows above 1.0 V two further irreversible oxidation steps. Since Ga^{III} and Cr^{III} in **1** and **4** are unlikely to undergo metal-centered redox reactions, we conclude that complexes **1** and **4** undergo ligand-centered

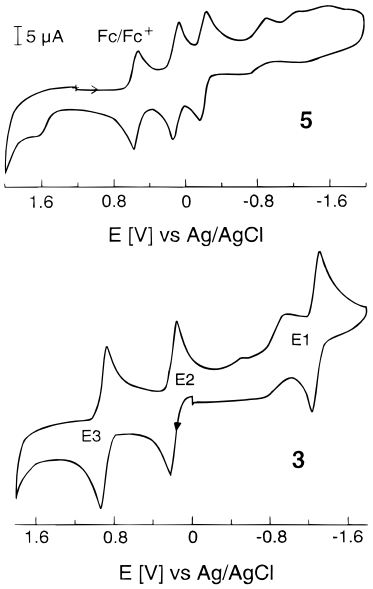

Figure 5. Cyclic voltammograms of **5** (top) and **3** (bottom) in CH_3CN, containing 0.10 M tetra-*n*-butylammonium hexafluorophosphate as supporting electrolyte. (Conditions: glassy carbon working electrode; Ag/AgCl (LiCl, C_2H_5OH) reference electrode; scan rate 100 mV s^{-1}.)

redox reactions with formation of thiyl radical intermediates at potentials >0.6 V *vs* Ag/AgCl. Interestingly, the CV of [LCo^{III}], **6**, exhibits a quasi-reversible one-electron oxidation at 0.55 V *vs* Ag/AgCl, which again is probably ligand centered, rather than an oxidation of Co^{III} to Co^{IV}. In the CV of [LFe^{III}], this one-electron oxidation wave is reversible at $E_{1/2} = 0.24$ V *vs* Ag/AgCl and may be metal centered, but a ligand-based oxidation cannot be ruled out. A reversible one-electron reduction of Fe^{III} to Fe^{II} is observed at −0.58 V.[14] The species [LNi]$^-$ displays a reversible one-electron oxidation at even lower potential ($E_{1/2} = -0.13$ V *vs* Ag/AgCl) which we assign to a metal-centered Ni^{II}/Ni^{III} couple and an irreversible oxidation at +0.18 V which is probably ligand centered. The CV of [LMn^{III}], **5**, displays two reversible one-electron transfer waves at $E_{1/2} = 0.10$ V and −0.18 V *vs* Ag/AgCl (Figure 5, top). Both are considered to be metal centered because **5a**, a genuine Mn^{IV} species, shows an identical CV:

$$[LMn^{IV}]^+ \underset{-e}{\overset{+e}{\rightleftharpoons}} [LMn^{III}] \underset{-e}{\overset{+e}{\rightleftharpoons}} [LMn^{II}]^- \qquad (5)$$

Both the [LMn^{IV}]$^+$ and [LMn^{II}]$^-$ species are stable on the time scale of a coulometric experiment: oxidation of **5** at a constant potential of 0.45 V *vs* Ag/AgCl produced 0.96 electron equiv, and reduction of **5** at −0.65 V *vs* Ag/AgCl required 0.92 equiv.

Figure 5 (bottom) shows the CV of [LV^{III}], **3**, in acetonitrile solution. Clearly, *three* reversible one-electron transfer waves are detected at $E_{1/2} = 0.89$, 0.20, and −1.24 V *vs* Ag/AgCl which are assigned as in eq 6. The CV of **3a** is identical. Both

$$[LV^{V}]^{2+} \underset{-e}{\overset{+e}{\rightleftharpoons}} [LV^{IV}]^+ \underset{-e}{\overset{+e}{\rightleftharpoons}} [LV^{III}] \underset{-e}{\overset{+e}{\rightleftharpoons}} [LV^{II}]^- \qquad (6)$$

oxidations of **3** were verified by coulometry first at a constant potential of 0.5 V and then at 1.1 V *vs* Ag/AgCl, which showed 0.98 and 0.92 electron equiv, respectively.

The electrochemistry of some of the dinuclear complexes was also investigated in acetonitrile solution (0.10 M tetra-*n*-butylammonium hexafluorophosphate) in the potential range +1.5 to −1.0 V *vs* Ag/AgCl. For the following complexes an irreversible, ligand-centered oxidation wave at E_p^{ox} *vs* Ag/AgCl potentials was observed: **9**, 0.68 V; **10**, 1.36 V; **13**, 0.97 V; **14**, 0.93 V; **16**, 0.71 V.

Discussion

The hexadentate trianionic ligand tris(4-*tert*-butyl-2-mercaptobenzyl)-1,4,7-triazacyclononane forms very stable six-coordinate mononuclear first-row transition metal complexes in the di-, tri-, tetra-, or pentavalent oxidation state and resembles in this respect its 1,4,7-tris(*o*-hydroxybenzyl)-1,4,7-triazacyclononane[4−7] and 1,4,7-tris(*o*-aminobenzyl)-1,4,7-triazacyclononane analogs.[11−13] For a given redox-active transition metal ion in a given oxidation state, e.g. M(III), there are accessible, in general, also the di- and tetravalent states or, as in the case of V(III), the pentavalent state provided that the d^n electron configuration of the metal ion permits this.

It is therefore interesting that metal ions with a d^0 electron configuration as in [LGa^{III}], **1**, or [Lln^{III}], **2**, are electrochemically irreversibly oxidizable at a potential of ∼1.0 V *vs* Ag/AgCl. This process is probably a two-electron process and can only be ligand centered. We propose that a coordinated disulfide ligand forms intramolecularly. We have as yet been unable to isolate and characterize such a species. Therefore, the above proposal is admittedly speculative.

It is remarkable that [LCo^{III}], **6**, cannot be reduced reversibly to the [Co^{II}L]$^-$ species. Only an irreversible reduction at −1.3 V *vs* Ag/AgCl is observed. This is a clear indication that the ligand L stabilizes the trivalent oxidation state enormously over the divalent one. On the other hand, **6** is quasi-reversibly one-electron oxidized to an [LCo]$^+$ species at 0.55 V *vs* Ag/AgCl, which is a less positive potential by ∼450 mV than that for the two-electron oxidation of **1**. Co(IV) in an N_3S_3 donor environment is probably not a readily accessible oxidation state, but it is conceivable that a coordinated thiyl radical is formed which on the time scale of a cyclic voltammetry experiment is not very stable. [LCr^{III}], **4**, is a species where the Cr(IV) oxidation state (in a N_3S_3 donor set) is also considered to be less readily accessible, and consequently, an irreversible (probably 2e) oxidation process is observed at 0.65 V *vs* Ag/AgCl. The corresponding tris(phenolato)chromium(III) analog of **4** undergoes a quasi-reversible one-electron oxidation at 0.81 V *vs* Ag/AgCl, which probably involves the formation of a coordinated phenoxyl radical species.[5] In **4**, the formation of a coordinated disulfide may be envisaged. The Cr(II) oxidation level is not accessible to −1.9 V *vs* Ag/AgCl.

As pointed out previously,[14] the most intriguing species is [LFe^{III}], which exhibits a reversible one-electron oxidation wave at as low a potential as 0.24 V *vs* Ag/AgCl. The nature of this process is unclear at this point, since the $E_{1/2}$ value is considered to be too low for a ligand-centered oxidation, but Fe(IV) is also an oxidation state which is generally not readily accessible. Note that the corresponding tris(phenolato)iron(III) complexes are *not* oxidizable in the potential range up to +0.90 V *vs* Ag/AgCl.[5] The Fe(II) oxidation level is accessible at −0.58 V for [LFe^{III}] and at −1.31 V *vs* Ag/AgCl for the corresponding tris(phenolato) species.[5] This is again an indication that the phenolato ligands dramatically stabilize the +III oxidation state as compared to their thiophenolato analogs.

For [LV^{III}] three metal-centered oxidation levels are available, namely V^V, V^{IV}, and V^{II}. The same holds for the tris(phenolato) derivative of vanadium(III), where the V^V/V^{IV} couple is observed at $E_{1/2} = +0.89$ V, the V^{IV}/V^{III} at −0.01, and the V^{III}/V^{II} at −1.90 V *vs* Ag/AgCl. Comparison with the corresponding redox potentials (Table 8) for [LV^{III}], **3**, shows an interesting trend. The electron-rich form, V^{II}, is more stable for the tris(thiophenolato) than for the tris(phenolato) form by 590 mV.

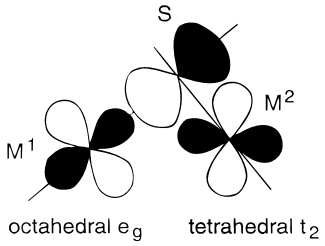

Figure 6. The orientation of a p orbital on sulfur with respect to e_g on an octahedral and t_2 on a tetrahedral metal ion in $[LM^1M^2Cl]$ complexes.

The V^{IV} form is stabilized in the N_3O_3 environment by 200 mV as compared to the N_3S_3 donor set, but this stabilization is already less pronounced than for the V^{II}/V^{III} forms. Interestingly, this difference between the redox potentials is nearly zero for the two V^V/V^{IV} couples. Thus, vanadium(V) with a d^0 electron configuration in an N_3O_3 or N_3S_3 environment is stabilized to the same extent.

Finally, for the metal-centered redox couples Mn^{IV}/Mn^{III} and Mn^{III}/Mn^{II} for [LMn], **5**, and its tris(phenolato) analog,[5] a similar picture emerges. The Mn^{III} redox level is more stable toward reduction for the N_3O_3Mn species than for the N_3S_3Mn complex **5** by 190 mV (**5** is more easily reduced) whereas the Mn^{IV} state is more stable in **5**, which is more easily oxidized by 160 mV as compared to its tris(phenolato) analog.[5]

The data in Table S2 deserve a comment. The ligand field parameters *Dq* and the Racah parameter *B* give insight into the strength of the σ- and π-donor bonds of a given complex. It is interesting that the values of *Dq* for octahedral complexes of cobalt(III) (d^6 low spin) and chromium(III) (d^3) containing the same pure σ-donor set (6 NH_3, 2 1,4,7-triazacyclononane) are always larger for the cobalt(III) complex. Thus, the difference $\Delta(Dq_{Co}-Dq_{Cr})$ for such pairs of complexes is positive and is in the range 110−140 cm^{-1} for the hexaaqua, hexaammine, and bis(1,4,7-triazacyclononane) complexes. Since these ligands are pure σ-donors, this behavior reflects an intrinsic difference between a Co^{III} and Cr^{III} ion (d^6 *vs* d^3 electron configuration). The ionic radius of octahedrally coordinated Co^{3+} (low spin) is smaller than that of Cr^{3+} (0.685 Å *vs* 0.755 Å).[34] It is therefore quite remarkable that this difference becomes even larger (240 cm^{-1}) for the tris(anionic) hexadentate ligand 1,4,7-tris(5-*tert*-butyl-2-hydroxybenzyl)-1,4,7-triazacyclononane[5] (tapt). This reflects the fact that the three coordinated phenolato groups in $[Cr(tapt)]^0$ are good π-donors which decrease the ligand field splitting *Dq* whereas in $[Co^{III}(tapt)]$ such π-donor bonds cannot contribute significantly because the t^6_{2g} subshell is filled. It appears then counterintuitive that this difference $\Delta(Dq_{Co}-Dq_{Cr})$ for complexes [LCo] and [LCr] is *negative* (−60 cm^{-1}); i.e. *Dq* for **6** is *smaller* than that for **4**. We take this as a clear indication that the three thiophenolato groups in $[LCr^{III}]$ have a much weaker π-donor capability than those in the oxygen analog [Cr(tapt)], which yields a relative stronger stabilization of the t_{2g} orbitals, resulting in a larger *Dq* value. The same conclusion was obtained above spectroscopically by analyzing the ligand-to-metal charge transfer bands in the visible region of $[LFe^{III}]$ and its oxygen analogue $[Fe^{III}(tapt)]$. Here a direct measure for the π-donor strength for $[LFe^{III}]$ was derived which was about half of that reported for tris(catecholato)iron(III) complexes.[27] In addition, the smaller Racah parameters for **4** and **6** as compared to their tris(phenolato) derivatives indicate a more pronounced covalency of the metal-to-sulfur σ-bonds.

The magnetic properties of the dinuclear complexes **7**−**9**, **15**, and **17**−**19** are interesting because they each contain two paramagnetic metal ions connected by three μ_2-thiophenolate bridges. In this face-sharing octahedral (prismatic)/tetrahedral arrangement, the two metal ions are quite close to each other at ∼2.9 Å, and consequently the M−S−M′ bridging angles are acute at ∼74°. For all of these complexes an intramolecular *antiferromagnetic* exchange coupling has been observed. This is remarkable, since in the linear trinuclear complex $Ni^{II}_3(acac)_6$, where acac represents the monoanion pentane-2,4-dionate and where two adjacent octahedral Ni^{II} ions ($S = 1$) are connected by three oxygen bridges of the acac ligands (face-sharing bioctahedral),[35] the coupling between adjacent Ni^{II} ions is *ferromagnetic*.[36] The authors have interpreted this in the framework of the Goodenough−Kanamori rules as arising predominantly from orthogonalities of the type $e_g||p_x\perp p_y||e_g$.[37] The notation used here follows that of Ginsberg in ref 37, where the e_g magnetic orbitals of the Ni^{II} ions overlap with filled p_x and p_y orbitals of the oxygen bridge. The orthogonality originates then from Ni−O−Ni angles close to 90°, at 84°. In the present dinuclear cases, the octahedral metal ion (Mn^{II}, Ni^{II}, Co^{II}) has two unpaired electrons in the e_g orbitals whereas the corresponding tetrahedral metal ion has two (Ni(II)) or three (Co(II), Fe(II)) unpaired electrons in the t_2 orbitals. Thus, the magnetic orbitals at the octahedral metal ion are half-filled e_g and at the tetrahedral ion are t_2 orbitals (in O_h and T_d symmetries, respectively). It is possible to orientate these magnetic metal orbitals to show a net overlap with a filled p orbital of the bridging sulfur, $e_g||p||t_2$, and consequently, a magnetic superexchange pathway leading to an antiferromagnetic exchange interaction is identifiable. This is shown in Figure 6. It is noted that this pathway is not available in the face-sharing bioctahedral case for two Ni(II) ions because then the t_{2g} orbitals are filled and a small ferromagnetic contribution results.

Acknowledgment. We thank the Fonds der Chemischen Industrie for financial support of this work.

Supporting Information Available: Table S1, containing fast atom bombardment mass spectroscopic data, Table S2, summarizing ligand field parameters, Table S3, containing elemental analysis data for new complexes, Figures S1 and S2, showing electronic absorption spectra of $[LV^{III}]$, $[LV^{IV}]^+$, and $[LV]^{2+}$ in CH_3CN and of **4**, **5**, and **5a** in $CHCl_3$, respectively, Figures S3 and S4, showing electronic spectra of **14** and **16** in $CHCl_3$ and of **13** and **18** in $CHCl_3$, respectively, Figures S5 and S6, showing the temperature dependence of the magnetic moments of **14** and **16** and of **18** and **19**, respectively, Figure S7, displaying cyclic voltammograms of **1** and **4**, and listings of crystallographic data, bond lengths and angles, anisotropic thermal parameters, and calculated positions of hydrogen atoms for complexes **6** and **14** (28 pages). Ordering information is given on any current masthead page.

IC951623U

(34) Shannon, R. D. *Acta Crystallogr*. **1976**, *A32*, 751.
(35) Bullen, G. J.; Mason, R.; Pauling, P. *Inorg. Chem*. **1965**, *4*, 456.
(36) (a) Ginsberg, A. P.; Martin, R. L.; Sherwood, R. C. *Inorg. Chem*. **1968**, *7*, 932. (b) Boyd, P. D. W.; Martin, R. L. *J. Chem. Soc., Dalton Trans*. **1979**, 92.
(37) Ginsberg, A. P. *Inorg. Chim. Acta Rev*. **1971**, *5*, 45.